



# Signatures of Surface Magnetic Disorder in Niobium Films

Alena S. Samsonova, Philipp I. Zolotov , Elmira M. Baeva, Andrey I. Lomakin, Nadezhda A. Titova, Anna I. Kardakova , and Gregory N. Goltsman

**Abstract**—We present our studies on the evolution of the normal and superconducting properties with thickness of thin Nb films with a low level of non-magnetic disorder ( $k_{Fl} \approx 150$  for the thickest film in the set). The analysis of the superconducting behavior points to the presence of magnetic moments, hidden in the native oxide on the surface of Nb films. Using the Abrikosov-Gorkov theory, we obtain the density of surface magnetic moments of  $10^{13} \text{ cm}^{-2}$ , which is in agreement with the previously reported data for Nb films.

**Index Terms**—Abrikosov-Gorkov model, superconducting thin films, superconducting transition temperature.

## I. INTRODUCTION

IN PRACTICAL applications, such as photon detection [1]–[4], sensitive magnetometry [5], or kinetic inductance based circuits [6], it is advantageous to reduce the volume or cross-sectional area of the active superconducting element, and so ultrathin superconducting films are commonly used. However, in the case of a decrease in film thickness below its characteristic length scale, such as the coherence length, one usually encounters a significant change in its superconducting properties. For most materials, the critical temperature ( $T_c$ ) decreases with film thickness, with rare exceptions like aluminum films [7]. Despite several decades of study of the thickness dependence of  $T_c$  for various materials, there is no universal explanation for this phenomenon, and the problem is usually resolved individually for each material.

Manuscript received November 30, 2020; revised January 25, 2021; accepted February 15, 2021. Date of publication March 11, 2021; date of current version May 20, 2021. This work was supported in part by the Russian Foundation for Basic Research under Contract 19-32-60076 (sample fabrication, and transport measurements), in part by the grant of the President RF No. MK-1308.2019.2. (Corresponding author: Anna Kardakova.)

Alena S. Samsonova is with Skolkovo Institute of Science and Technology (Skoltech), 121205 Moscow, Russia (e-mail: alena\_samsonova@outlook.com).

Philipp I. Zolotov is with the Moscow State Pedagogical University, 119991 Moscow, Russia, with the National Research University Higher School of Economics, 101000 Moscow, Russia, and with LLC Superconducting Nanotechnology (SCONTEL), 119021 Moscow, Russia (e-mail: fzolotov@hse.ru).

Elmira M. Baeva and Andrey I. Lomakin are with the National Research University Higher School of Economics, 101000 Moscow, Russia (e-mail: baeva.elm@gmail.com; andrey.lomakin.2021@mail.ru).

Nadezhda A. Titova is with Moscow State Pedagogical University, 119991 Moscow, Russia (e-mail: titovana@mail.ru).

Anna I. Kardakova and Gregory N. Goltsman are with the National Research University Higher School of Economics, 101000 Moscow, Russia and with Moscow State Pedagogical University, 119991 Moscow, Russia (e-mail: akardakova@hse.ru; ggoltsman@hse.ru).

Color versions of one or more figures in this article are available at <https://doi.org/10.1109/TASC.2021.3065281>.

Digital Object Identifier 10.1109/TASC.2021.3065281

Thin Nb films are one of the most widely used materials in superconducting electronic applications [8]. The properties of thin Nb films have been addressed by numerous studies, with particular emphases on the dependence of  $T_c$  on the film thickness [9]–[17]. These studies show that the deposition process and the substrate material strongly influence the  $T_c$ . As already shown, the Nb films, grown on R-cut sapphire substrates, have superior superconducting properties [14]. Despite that superconductivity retains in high quality Nb films down to thicknesses of several monoatomic layers, the critical temperature is strongly suppressed with decreasing thickness. For conventional metallic superconductor,  $T_c$  is considered to be independent of the degree of elastic scattering [18], and different mechanisms are proposed to explain the suppression of  $T_c$  in high-quality Nb films. For example, higher density of defects or strain effects in thin films may influence the  $T_c$  due to modification of the electron-electron and the electron-phonon interactions [9], [11], [16]. In addition, a predisposition of Nb films to rapid oxidization is known to enhance the drop of  $T_c$  in ultrathin films [19]. Besides reduction of effective film thickness, an oxide layer, formed on the film surface, may suppress  $T_c$  due to its specific properties. On the one hand, non-stoichiometric oxides of Nb are known to be conductive [20], and  $T_c$  can be suppressed as a result of inverse proximity effect [14], [17]. On the other hand, the oxide layer may possess magnetic disorder that suppresses superconducting properties due to the spin-flip scattering [21], [22].

Here we focus on the study of Nb films grown on R-cut sapphire, which demonstrate excellent metallic properties down to thicknesses of 2.5 nm. In the following, we study the superconducting properties and consider several mechanisms that may cause to the suppression of the  $T_c$  with decreasing film thickness. Analysis of the experimental data in the framework of the Abrikosov-Gorkov model [23] shows that a very small amount of magnetic disorder can strongly suppress  $T_c$  in high-quality ultrathin Nb films.

## II. EXPERIMENTAL METHODS

### A. Magnetron Sputtering of High-Ordered Nb Films

High-quality Nb films are grown on the 400  $\mu\text{m}$ -thick substrate by magnetron sputtering. The basic pressure in the main chamber is  $\sim 8 \times 10^{-8}$  Torr. To achieve a contaminant-free atmosphere during the process, Ti target is presputtered for 5 minutes to cover the chamber surfaces with titanium layer and lower the pressure down to  $\sim 2 \times 10^{-8}$  Torr. During presputtering the

TABLE I  
THE PARAMETERS OF Nb FILMS

$d$ (nm)	$T_c$ (K)	$R_{sq,300K}$ ( $\Omega/\text{sq}$ )	$RRR$	$D$ ( $\text{cm}^2/\text{s}$ )	$l$ (nm)	$\xi$ (nm)
62	9.2	2.3	25	10.4	11.4	17.8
26	8.8	6.2	9	6.5	7.1	14.4
10	8.4	21.5	6.1	3.5	3.9	11.9
6	6.5	57	1.3	2.4	2.6	12.5
4	5.1	116	0.7	-	-	-
6*	7.1	41	2.7	3.1	3.5	11.4
4*	4.4	105	0.7	1.6	1.8	13.3
2.5*	2.4	203	0.3	0.5	0.5	9.9

wafers are protected by an inbuilt shutter. The deposition of Nb films is performed in the DC regime at 600 mA by sputtering the high purity (3N5) 2-inch Nb target and depositing material onto a rotating substrate holder. During the deposition process the substrate is heated up to 400 °C. After heating the substrates to the desired temperature, high purity (4N8) argon gas is led into the chamber at a constant flow rate of 40 sccm resulting in the working pressure of 3.1 mTorr. The plasma discharge is then turned on and stabilized for 5 minutes. After that, the shutter is opened, and the film is with the deposition rate about 0.077 nm/s. After turning off the discharge, the substrates are cooled down in a vacuum for 2 hours, and then they are pulled out of the vacuum. Additionally, the thinnest samples, marked in Table I with \*-symbol, are covered *in situ* with a 1-nm Ti-layer. Under atmospheric conditions, the Ti layer transforms to oxide,  $TiO_x$ , and prevents fast oxidation of the ultrathin Nb film in air.

### B. The Measurement of the Metal Properties of Nb Films

The electrical and superconducting properties of Nb films were investigated on unpatterned samples immediately after the fabrication. Transport measurements were performed on the Nb Hall-bar structures of 500  $\mu\text{m}$  wide and 1000  $\mu\text{m}$  long. All measurements were performed using the low-frequency AC technique in a four-probe configuration. The applied bias currents were less than 1  $\mu\text{A}$ . The measurements were carried out in a  $^4\text{He}$  cryogenic insert (LLC Scontel), immersed in a dewar vessel, in a wide temperature range (from 300 K to 1.7 K). The critical temperature  $T_c$  was determined as the temperature at which the film has lost half of its resistance,  $R = 0.5R_0$ , where  $R_0$  is the normal state resistance just above the superconducting transition. The measurements of the Hall effect and upper critical magnetic field  $B_{c2}$  were performed in a perpendicular magnetic field ( $B$ ) in the Hall-bar structures. Using the Hall resistance  $R_H$  at  $T = 10$  K, the carrier density  $n_0$  was found as  $n_0 = R_H/(eBd)$ . From the measurements of the temperature dependencies of  $R(T)$  at different values of the perpendicular magnetic field, the slope of the upper critical magnetic field  $dB_{c2}/dT$  at  $T_c$  was determined. The latter was used to estimate the electron diffusivity constant  $D = -4k_B/(\pi e)(dB_{c2}/dT)^{-1}$  and the Ginzburg-Landau coherence length  $\xi_{GL}^2(0) = -\Phi_0(dB_{c2}/dT)^{-1}/(2\pi T_c)$ , where  $\Phi_0$  is the magnetic flux quantum.

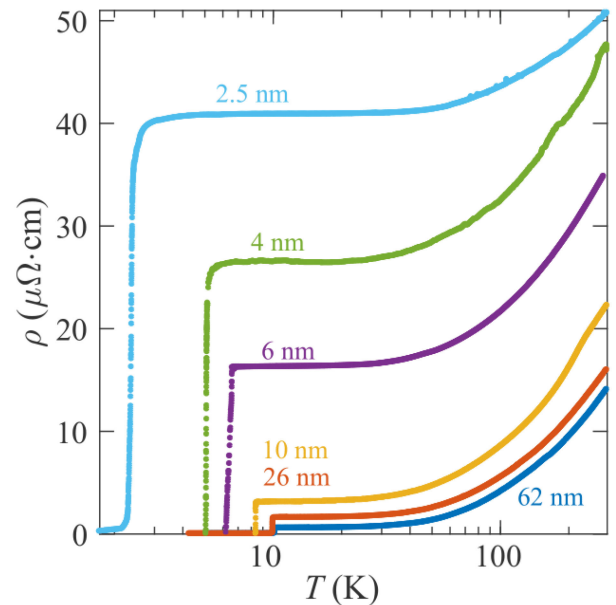


Fig. 1. Temperature dependence of the resistivity  $\rho(T)$  for Nb films with a thickness ranging from 2.5 nm to 62 nm. The results for  $\rho(T)$  are presented mainly for the Nb films without the capping layer, with the exception for the film with a thickness of 2.5 nm.

### III. RESULTS AND DISCUSSION

To characterize the electrical properties of the samples, we determine the resistivity ( $\rho$ ) and the residual resistance ratio ( $RRR$ ) as  $\rho = R_{sq}d$  and  $RRR = (R_{sq,300K} - R_{sq,10K})/R_{sq,10K}$ , where  $R_{sq}$  is the resistance per square,  $d$  is the film thickness (see Table I for details). Figure 1 shows the temperature dependencies of resistivity  $\rho(T)$  for the Nb films of different thicknesses in a 300 – 1.7 K temperature range. As a function of the decreasing temperature,  $\rho \propto T$  decreases linearly at high temperatures, over a wide range between 50 K and 300 K, and then, at approximately  $T = 20$  K, it reaches a residual value,  $\rho_0$ . Upon further cooling,  $\rho(T)$  drops down to zero resistance below the critical temperature. For thinner films the residual resistivity  $\rho_0$  increases and the  $T_c$  decreases.

Analysis of the dependence of resistivity on film thickness can provide an additional information about the film structure. The linear temperature dependence of  $\rho$  at high temperatures is typical for metals and usually due to electron-phonon scattering [24]. Figure 2 shows the contribution of the electron-phonon coupling to the conductivity of Nb films at room temperature, which is designated as  $G_{ph} = (R_{300K} - R_{10K})^{-1}$ . The phonon conductance  $G_{ph}$ , as expected, linearly decreases with the film thickness. However, as shown with the dashed line in Figure 2, it approaches zero at some thickness, approximately  $d_{dl} \approx 2.1 \pm 0.5$  nm. This thickness, called the “dead” layer, is presumably related to a native oxide on the surface of the Nb films, which mainly consists of non-conductive niobium oxide ( $\text{Nb}_2\text{O}_5$ ) [25], [26]. At a temperature of 10 K, the effect of electron-phonon scattering becomes negligible, and an analysis

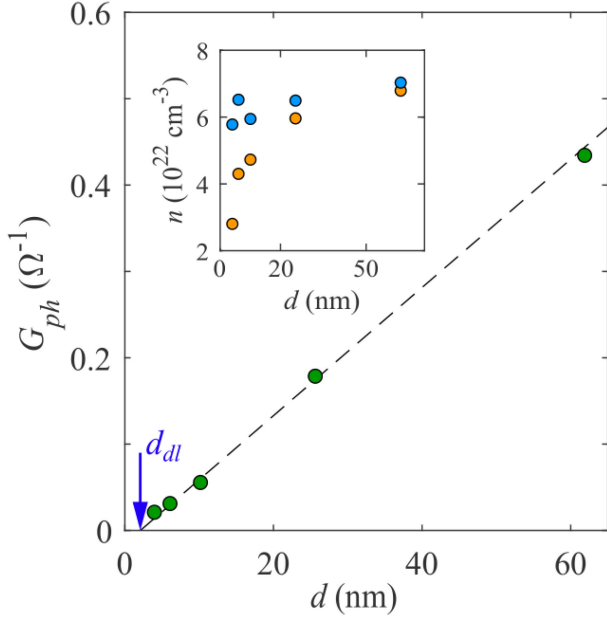


Fig. 2. Normal state properties of the Nb films. The data is presented for films without the capping layer. Main body: the thickness-dependent phonon conductance at 300 K:  $G_{ph} = (R_{300K} - R_{10K})^{-1}$ . The dashed line shows the linear dependence of  $G_{ph}(d)$  on the film thickness. Here, the point of intersection of the fit with the x-axis defines the thickness of a non-conducting oxide layer on the top of Nb films ( $d_{dl} = 2.1 \pm 0.5$  nm). Inset: the carrier density in Nb films as a function of film thickness. The carrier density  $n$  is determined from the Hall effect measurements as  $n_0 = R_H/(eBd)$ , where  $R_H$  is the Hall resistance at  $T = 10$  K. The raw data for  $n_0$  are shown with the orange circles. The data, plotted with the blue circles, are obtained taking into account the non-conducting oxide layer, as  $n^* = n_0 d/(d - d_{dl})$  with  $d_{dl} = 2.1$  nm.

of the dependence  $\rho_0(d)$  suggests additional scattering mechanisms contributing to resistance, such as scattering at impurities, grains, and film boundaries.

Taking into account the thickness of the dead layer, we characterize other electronic parameters of the Nb films such as the carrier density at low temperatures. The hole-type carrier density as a function of  $d$  is presented in the inset of Fig. 2: the raw data,  $n_0$ , and the revised data,  $n^* = n_0 d/(d - d_{dl})$ , are shown with the orange and blue circles, respectively. Due to the revision of the film thickness, we observe that the carrier density does not significantly change and remains close to the value of  $n_0 = 6.7 \times 10^{22} \text{ cm}^{-3}$ , obtained for the 60-nm Nb film. This finding suggests that the electronic properties in Nb films are persistent to a change in the film thickness.

To characterize the degree of non-magnetic disorder in the Nb films, we estimate important microscopic parameters, such as the electron mean free path  $l$  and the coherence length  $\xi$ . The mean free path  $l$  in Nb films is estimated using the experimental values of the electron diffusivity,  $D$ , as  $l = 3D/v_F$ , where  $v_F = 2.73 \times 10^5$  m/s is the Fermi velocity in Nb [27]. The values of  $\xi$ , found from the slopes of the upper critical magnetic field, scale from 18 nm to 10 nm for Nb films of 60 nm and 2.5 nm, respectively. It worth mentioning that the values of  $l$ , found for the Nb samples thicker than 6 nm, are in agreement with the estimates of  $\xi$  in the dirty limit:  $\xi = 0.852\sqrt{\xi_0 l}$ , where Nb bulk coherence length  $\xi_0 = 38$  nm [27]. The above parameters of the

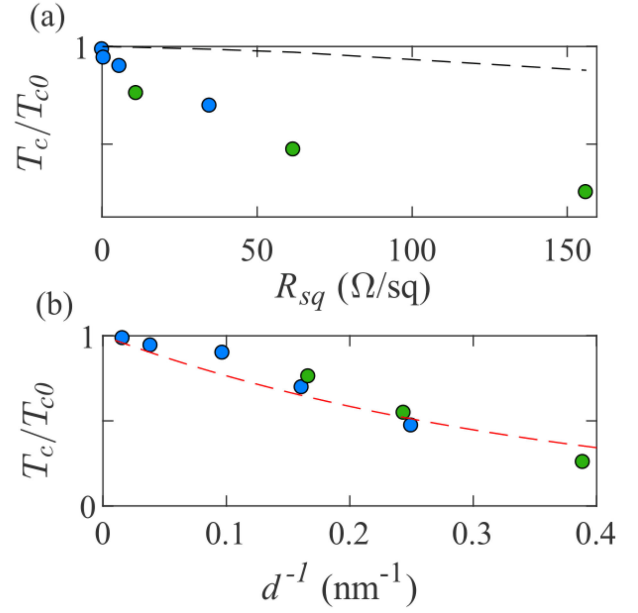


Fig. 3. (a) The normalized critical temperature  $T_c/T_{c0}$  as function of the resistance per square  $R_{sq}$ . The circles represent the experimental data, the black dashed line represents predictions of the Finkelstein model [28] (Eq. 1). (b) The normalized critical temperature  $T_c/T_{c0}$  as function of the inverse thickness  $d^{-1}$ . The circles represent the experimental data for the Nb films, and the red dashed line shows the fit with the McMillan model [29] (Eq. 2), supposing that  $d_N = 0.8 \pm 0.2$  nm. The samples without the capping layer and covered with the TiO<sub>x</sub> layer are shown with blue and green circles, respectively.

studied Nb films are summarized in Table I, where the data for the samples with the TiO<sub>x</sub> capping layer are marked with \*-symbol. We believe that the studied Nb samples are of high quality, as evidenced by the relatively large value of the Ioffe-Regel parameter, which can be estimated as  $k_F l = (3\pi^2 n_0)^{1/3} l \approx 150$  for the thick film. In addition, the samples with the TiO<sub>x</sub> capping layer exhibit better electronic and superconducting properties compared to the uncoated samples.

Next, we analyze the suppression of the  $T_c$  in the framework of the weak disorder model [28], in which impurities reinforce Coulomb interactions.  $T_c$  is expressed as a function of the resistance per square  $R_{sq}$  and the elastic scattering time  $\tau$ :

$$\frac{T_c}{T_{c0}} = e^{\gamma} \left( \frac{1/\gamma - \sqrt{t/2} + t/4}{1/\gamma + \sqrt{t/2} + t/4} \right)^{1/\sqrt{2t}}, \quad (1)$$

where  $\gamma = \ln(h/k_B T_{c0} \tau)$  and  $t = R_{sq} e^2 / \pi h$ . In Fig. 3(a) we plot the normalized critical temperature  $T_c/T_{c0}$  as a function of  $R_{sq}$ , where  $T_{c0} = 9.35$  K taken as the critical temperature of bulk niobium. As shown in Fig. 3(a), the theoretical prediction of the model, which takes into account the experimental values of  $R_{sq}$  and  $\tau = l^2/(3D)$ , does not describe the observed suppression of  $T_c$  in the Nb films. Thus, the effect of the non-magnetic disorder on  $T_c$  can be neglected in these films.

As a relevant mechanism for suppression of  $T_c$  in thin Nb films is commonly considered the inverse proximity effect due to a presence of the non-superconducting layer on the film surface or at interface of the film and the substrate [14], [17], [29], [30].

The critical temperature is depressed as a function of thickness according to the relation:

$$T_c = T_{c0} \left( \frac{3.56\Theta_D}{T_{c0}} \right)^{-\alpha/d}. \quad (2)$$

Here  $\alpha = d_N N_N(0)/N_S(0)$ , where  $d_N$  is the thickness of the normal layer and  $N_N(0)/N_S(0)$  is the ratio of the densities of states in a normal metal and a superconductor. For simplicity,  $N_N(0)/N_S(0)$  is assumed to be 1. Fig. 3(b) presents the  $T_c/T_{c0}$  as a function of the inverse thickness  $d^{-1}$ , where the blue symbols represent the experimental data for the Nb films. We find that the full set of data can be described by the model with  $d_N = 0.8 \pm 0.2$  nm. Despite the obvious agreement between theory and experiment, we question the conductivity of the capping layer. First of all, the surface oxide layer consists mainly of  $\text{Nb}_2\text{O}_5$ , which exhibits insulating properties [25], [26]. We also eliminate the change in the charge density due to the observed trend with thickness decrease (see the inset in Fig. 2). Therefore, we conclude that the inverse proximity effect cannot be a primary mechanism of the  $T_c$  suppression in the studied Nb films.

Meanwhile, the niobium oxide is suspected to contain a small density of magnetic moments [21], [22], which can be detrimental for superconductivity in thin Nb films. In this case, the observed suppression of  $T_c$  with decreasing thickness may be explained by the interaction of Cooper pairs with the localized spins of the magnetic moments (spin-flip interactions) [23]. The spin-flip scattering time  $\tau_s$  and critical temperature  $T_c$  are related via the notorious Abrikosov-Gorkov equation:

$$\ln \left( \frac{T_{c0}}{T_c} \right) = \psi \left( \frac{1}{2} + \frac{\hbar}{2\pi k_B T_{c0} \tau_s} \right) - \psi \left( \frac{1}{2} \right). \quad (3)$$

Here,  $\psi$  is the digamma function,  $T_{c0}$  is the critical temperature in the absence of magnetic moments. Fig. 4 illustrates the dependence of the spin-flip scattering time  $\tau_s$  on the inverse thickness  $d^{-1}$ . The spin-flip scattering time decreases as the thickness decreases, which may confirm the predominance of surface magnetic moments in thin films. Considering the case of  $d < \xi$ , when the superconductivity is sensitive to the total volume density of the magnetic scatterers regardless of their distribution within the cross-section of the film, we use a simplified theoretical model that gives a quantitative description of the density of magnetic moments. The dependence  $\tau_s^{-1}(d^{-1})$  shown in Fig. 4 allows to determine the effective density of magnetic moments  $N_M$ , including the contributions of surface magnetic moments  $N_s$  and magnetic moments in bulk  $N_b$ . The relation between these two quantities is given by  $N_M = N_s(a/d) + N_b$ . At the same time,  $N_M \sim a/v_F\tau_s$ , where  $a = 0.33$  nm is the lattice constant for Nb [14]. The analysis of  $\tau_s^{-1}(d^{-1})$  dependence provides with  $N_s = (9.5 \pm 1.9) \times 10^{-3}$  and  $N_b = 0$ , that corresponds to density of surface magnetic moments  $N_s a^{-2} = (8.6 \pm 0.8) \times 10^{12} \text{ cm}^{-2}$ . The estimated density of surface magnetic moments is in agreement with the previously reported results for Nb films ( $\approx 5 \times 10^{13} \text{ cm}^{-2}$  [21], [31]–[33]). The experiments [22] also suggest that the native oxide in Nb is intrinsically defective, and substoichiometric  $\text{Nb}_2\text{O}_5$  produces unscreened  $d$ -band magnetic moments [20].

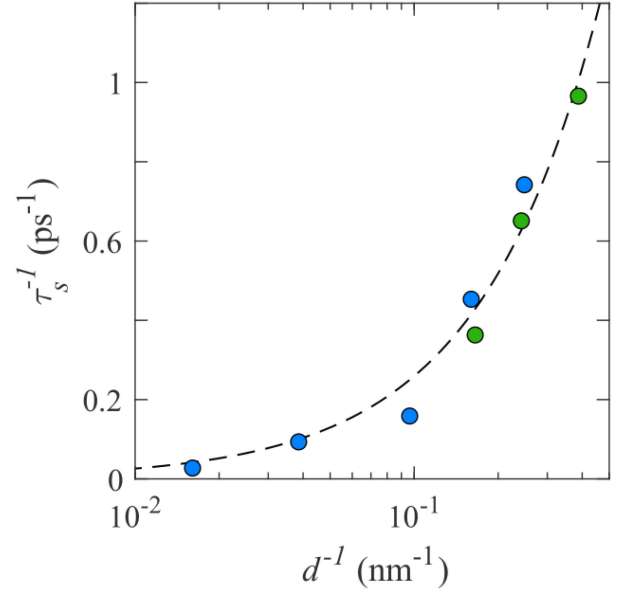


Fig. 4. A pair-breaking scattering rate as a function of inverse thickness ( $\tau_s^{-1}$  vs.  $d^{-1}$ ). The fitting of the data with the Eq. 3 demonstrates that the dominant contribution to the spin-flip scattering in thin films originates from the near-surface magnetic disorder. The samples without the capping layer and covered with the TiOx layer are shown with blue and green circles, respectively.

These defects are considered as potential candidates of magnetic disorder in niobium.

In our previous work, the analysis of the dependence of  $T_c(d)$  also points to the problem of surface magnetic disorder in ultrathin epitaxial TiN films [34]. Similar to the observations in copper [35] and aluminum [33], [36], the origin of surface magnetic disorder can be associated with oxygen vacancies in defective oxides. Some studies [22], [36], [37] show that the reduction of oxygen vacancies with the annealing treatment could reduce the density of the localized magnetic moments and, consequently, the scattering mechanism of magnetic moments with conduction electrons. The latter manifests itself in some improvement of superconducting properties. Thus, we assume that the further progress in fabrication of ultrathin films (such as Nb films) may be related with the surface treatment, aimed to prevent the formation of defective oxides on film surface.

#### IV. CONCLUSION

The research is devoted to the study of superconducting and transport properties of ultrathin Nb films, grown on R-plane sapphire substrate. The analysis of the superconducting behavior points to the presence of magnetic moments. The computed parameters of the density of surface magnetic moments ( $N_s a^{-2} \approx 10^{13} \text{ cm}^{-2}$ ) agree with the previously reported results for niobium films.

#### ACKNOWLEDGMENT

The authors would like to acknowledge V. Khrapai and A. Semenov for useful discussion of this article.

## REFERENCES

- [1] P. J. Burke *et al.*, "Length scaling of bandwidth and noise in hot-electron superconducting mixers," *Appl. Phys. Lett.*, vol. 68, no. 23, pp. 3344–3346, 1996.
- [2] A. J. Annunziata *et al.*, "Niobium superconducting nanowire single-photon detectors," *IEEE Trans. Appl. Supercond.*, vol. 19, no. 3, pp. 327–331, Jun. 2009.
- [3] R. Barends *et al.*, "Niobium and tantalum high Q resonators for photon detectors," *IEEE Trans. Appl. Supercond.*, vol. 17, no. 2, pp. 263–266, Jun. 2007.
- [4] K. Inderbitzin, A. Engel, A. Schilling, K. Ilin, and M. Siegel, "An ultrafast superconducting Nb nanowire single-photon detector for soft x-rays," *Appl. Phys. Lett.*, vol. 101, Oct. 2012, Art. no. 162601.
- [5] L. Chen, H. Wang, X. Liu, L. Wu, and Z. Wang, "A high-performance Nb nano-superconducting quantum interference device with a three-dimensional structure," *Nano Lett.*, vol. 16, pp. 7726–7730, Nov. 2016.
- [6] A. J. Annunziata *et al.*, "Tunable superconducting nanoinductors," *Nanotechnology*, vol. 21, Oct. 2010, Art. no. 445202.
- [7] K. Y. Arutyunov *et al.*, "Quantum size effect in superconducting aluminum films," *Phys. Solid State*, vol. 61, no. 9, pp. 1559–1562, 2019.
- [8] A. I. Braginski, "Superconductor electronics: Status and outlook," *J. Supercond. Novel Magnetism*, vol. 32, no. 1, pp. 23–44, 2019.
- [9] C. C. Koch, J. O. Scarbrough, and D. M. Kroeger, "Effects of interstitial oxygen on the superconductivity of niobium," *Phys. Rev. B*, vol. 9, pp. 888–897, Feb. 1974.
- [10] J. H. Quate, "T<sub>c</sub> suppression and critical fields in thin superconducting Nb films," *Phys. Rev. B*, vol. 34, pp. 1948–1951, Aug. 1986.
- [11] E. Gershenzon, M. Gershenzon, G. Gol'tsman, A. Lyul'kin, A. Semeniv, and A. Sergeev, "Electron-phonon interaction in ultrathin Nb films," *Sov. Phys. JETP*, vol. 70, pp. 505–511, Mar. 1990.
- [12] S. Bose, P. Raychaudhuri, R. Banerjee, P. Vasa, and P. Ayyub, "Mechanism of the size dependence of the superconducting transition of nanostructured Nb," *Phys. Rev. Lett.*, vol. 95, Sep. 2005, Art. no. 147003.
- [13] Y. Jin, X. Song, and D. Zhang, "Grain-size dependence of superconductivity in dc sputtered Nb films," *Sci. China Ser. G: Phys., Mechanics Astron.*, vol. 52, pp. 1289–1292, Aug. 2009.
- [14] C. Delacour *et al.*, "Persistence of superconductivity in niobium ultrathin films grown on r-plane sapphire," *Phys. Rev. B*, vol. 83, Apr. 2011, Art. no. 144504.
- [15] X. Q. Jia *et al.*, "High performance ultra-thin niobium films for superconducting hot-electron devices," *IEEE Trans. Appl. Supercond.*, vol. 23, no. 3, Jun. 2013, Art. no. 2300704.
- [16] I. Zaytseva *et al.*, "Negative hall coefficient of ultrathin niobium in Si/Nb/Si trilayers," *Phys. Rev. B*, vol. 90, Aug. 2014, Art. no. 060505.
- [17] N. Pinto *et al.*, "Dimensional crossover and incipient quantum size effects in superconducting niobium nanofilms," *Sci. Rep.*, vol. 8, no. 1, pp. 1–12, Mar. 2018.
- [18] P. Anderson, "Theory of dirty superconductors," *J. Phys. Chem. Solids*, vol. 11, no. 1, pp. 26–30, 1959.
- [19] D. F. Santavica and D. E. Prober, "Aging of ultra-thin niobium films," *IEEE Trans. Appl. Supercond.*, vol. 25, no. 3, Jun. 2015, Art. no. 2200104.
- [20] R. J. Cava *et al.*, "Electrical and magnetic properties of Nb<sub>2</sub>O<sub>5-δ</sub> crystallographic shear structures," *Phys. Rev. B*, vol. 44, pp. 6973–6981, Oct. 1991.
- [21] A. Rogachev, T.-C. Wei, D. Pekker, A. T. Bollinger, P. Goldbart, and A. Bezryadin, "Magnetic-field enhancement of superconductivity in ultranarrow wires," *Phys. Rev. Lett.*, vol. 97, 2006, Art. no. 137001.
- [22] T. Proslir *et al.*, "Tunneling study of cavity grade Nb: Possible magnetic scattering at the surface," *Appl. Phys. Lett.*, vol. 92, May 2008, Art. no. 212505.
- [23] A. A. Abrikosov and L. P. Gor'kov, "Contribution to the theory of superconducting alloys with paramagnetic impurities," *Sov. Phys. JETP*, vol. 12, no. 6, pp. 1243–1263, Dec. 1961.
- [24] J. M. Ziman, *Electrons and Phonons: The Theory of Transport Phenomena in Solids*. New York: Oxford Univ. Press, 2001.
- [25] C. Nico, T. Monteiro, and M. Graça, "Niobium oxides and niobates physical properties: Review and prospects," *Prog. Mater. Sci.*, vol. 80, pp. 1–37, 2016.
- [26] A. V. Lubchenko *et al.*, "Xps study of niobium and niobium-nitride nanofilms," *J. Surf. Investigation: X-ray, Synchrotron Neutron Techn.*, vol. 12, pp. 1819–7094, 2018.
- [27] H. R. Kerchner, D. K. Christen, and S. T. Sekula, "Critical fields  $H_c$  and  $H_{c2}$  of superconducting niobium," *Phys. Rev. B*, vol. 24, pp. 1200–1204, Aug. 1981.
- [28] A. Finkel'stein, "Suppression of superconductivity in homogeneously disordered systems," *Physica B: Condens. Matter*, vol. 197, pp. 636–648, Mar. 1994.
- [29] W. L. McMillan, "Tunneling model of the superconducting proximity effect," *Phys. Rev.*, vol. 175, pp. 537–542, Nov. 1968.
- [30] A. I. Gubin, K. S. Il'in, S. A. Vitusevich, M. Siegel, and N. Klein, "Dependence of magnetic penetration depth on the thickness of superconducting Nb thin films," *Phys. Rev. B*, vol. 72, no. 6, Aug. 2005, Art. no. 064503.
- [31] R. H. Koch, D. P. DiVincenzo, and J. Clarke, "Model for 1/f Flux noise in SQUIDS and qubits," *Phys. Rev. Lett.*, vol. 98, Jun. 2007, Art. no. 267003.
- [32] S. Sendelbach, D. Hover, M. Mück, and R. McDermott, "Complex inductance, excess noise, and surface magnetism in dc SQUIDS," *Phys. Rev. Lett.*, vol. 103, no. 11, Sep. 2009, Art. no. 117001.
- [33] P. Kumar *et al.*, "Origin and reduction of 1/f magnetic flux noise in superconducting devices," *Phys. Rev. Appl.*, vol. 6, no. 4, Oct. 2016, Art. no. 041001.
- [34] N. Saveskul *et al.*, "Superconductivity behavior in epitaxial TiN films points to surface magnetic disorder," *Phys. Rev. Appl.*, vol. 12, Nov. 2019, Art. no. 054001.
- [35] F. Pierre, A. B. Gougam, A. Anthore, H. Pothier, D. Esteve, and N. O. Birge, "Dephasing of electrons in mesoscopic metal wires," *Phys. Rev. B*, vol. 68, Aug. 2003, Art. no. 085413.
- [36] C. Barone *et al.*, "Kondo-like transport and magnetic field effect of charge carrier fluctuations in granular aluminum oxide thin films," *Sci. Rep.*, vol. 8, no. 1, 2018, Art. no. 13892.
- [37] S. E. de Graaf *et al.*, "Suppression of low-frequency charge noise in superconducting resonators by surface spin desorption," *Nature Commun.*, vol. 9, no. 1, pp. 1143 (1–6), Mar. 2018.